

X-ray photoelectron spectroscopy for identification of morphological defects and disorders in graphene devices

Pinar Aydogan, Emre O. Polat, Coskun Kocabas, and Sefik Suzer

Citation: *Journal of Vacuum Science & Technology A* **34**, 041516 (2016); doi: 10.1116/1.4954401

View online: <http://dx.doi.org/10.1116/1.4954401>

View Table of Contents: <http://scitation.aip.org/content/avs/journal/jvsta/34/4?ver=pdfcov>

Published by the AVS: Science & Technology of Materials, Interfaces, and Processing

Articles you may be interested in

Charge transfer effects in electrocatalytic Ni-C revealed by x-ray photoelectron spectroscopy

Appl. Phys. Lett. **100**, 231601 (2012); 10.1063/1.4722785

Influence of impurities on the x-ray photoelectron spectroscopy and Raman spectra of single-wall carbon nanotubes

J. Chem. Phys. **127**, 154713 (2007); 10.1063/1.2796153

The Purification of Single-Walled Carbon Nanotubes studied by X-ray induced Photoelectron Spectroscopy

AIP Conf. Proc. **685**, 120 (2003); 10.1063/1.1628000

Comparison of infrared, Raman, photoluminescence, and x-ray photoelectron spectroscopy for characterizing arc-jet-deposited diamond films

J. Appl. Phys. **83**, 4421 (1998); 10.1063/1.367201

X-ray photoelectron spectroscopy and x-ray diffraction study of the thermal oxide on gallium nitride

Appl. Phys. Lett. **70**, 2156 (1997); 10.1063/1.118944


Instruments for Advanced Science

<p>Contact Hiden Analytical for further details: W www.HidenAnalytical.com E info@hiden.co.uk</p> <p>CLICK TO VIEW our product catalogue</p>	 <p>Gas Analysis</p> <ul style="list-style-type: none"> › dynamic measurement of reaction gas streams › catalysis and thermal analysis › molecular beam studies › dissolved species probes › fermentation, environmental and ecological studies 	 <p>Surface Science</p> <ul style="list-style-type: none"> › UHV TPD › SIMS › end point detection in ion beam etch › elemental imaging - surface mapping 	 <p>Plasma Diagnostics</p> <ul style="list-style-type: none"> › plasma source characterization › etch and deposition process reaction › kinetic studies › analysis of neutral and radical species 	 <p>Vacuum Analysis</p> <ul style="list-style-type: none"> › partial pressure measurement and control of process gases › reactive sputter process control › vacuum diagnostics › vacuum coating process monitoring
--	--	--	--	--

X-ray photoelectron spectroscopy for identification of morphological defects and disorders in graphene devices

Pinar Aydoğan

Department of Chemistry, Bilkent University, 06800 Ankara, Turkey

Emre O. Polat and Coskun Kocabas

Department of Physics, Bilkent University, 06800 Ankara, Turkey

Sefik Suzer^{a)}

Department of Chemistry, Bilkent University, 06800 Ankara, Turkey

(Received 22 February 2016; accepted 9 June 2016; published 22 June 2016)

The progress in the development of graphene devices is promising, and they are now considered as an option for the current Si-based electronics. However, the structural defects in graphene may strongly influence the local electronic and mechanical characteristics. Although there are well-established analytical characterization methods to analyze the chemical and physical parameters of this material, they remain incapable of fully understanding of the morphological disorders. In this study, x-ray photoelectron spectroscopy (XPS) with an external voltage bias across the sample is used for the characterization of morphological defects in large area of a few layers graphene in a chemically specific fashion. For the XPS measurements, an external +6 V bias applied between the two electrodes and areal analysis for three different elements, C1s, O1s, and Au4f, were performed. By monitoring the variations of the binding energy, the authors extract the voltage variations in the graphene layer which reveal information about the structural defects, cracks, impurities, and oxidation levels in graphene layer which are created purposely or not. Raman spectroscopy was also utilized to confirm some of the findings. This methodology the authors offer is simple but provides promising chemically specific electrical and morphological information. © 2016 American Vacuum Society. [<http://dx.doi.org/10.1116/1.4954401>]

I. INTRODUCTION

In recent years, the new material graphene that is composed of a single or a few layer(s) of sp^2 hybridized pure carbon atoms arranged in a regular hexagonal honeycomb pattern gained an increasing interest for many research fields due to its unique mechanical, electrical, chemical, and thermal properties.^{1,2} Furthermore, it provides an ideal base for many electronic systems.³

For chemical characterization of graphene, numerous common tools, such as IR, UV-vis, Raman, and electron spectroscopic, electron and scanning-probe microscopic techniques have been extensively used. Among them, Raman spectroscopy is a convenient and well-established one to analyze graphene and its derivatives. Using this method, it has been claimed that both quality of synthesized graphene layer and number of (a few) layers can be identified by comparing the intensity ratios of two main features G and 2D in the spectra.⁴ Additionally, the presence of D and D' bands in the Raman spectrum, which are also called defect activated bands, indicates the change in sp^2 hybridized structure of graphene.⁵⁻⁷ Hence, Raman spectroscopy can also give information about defects, impurities, oxidation, etc.^{8,9} The nondestructive nature of the technique is also an advantage. On the other hand, conventional Auger and x-ray photoelectron spectroscopic (XPS) analyses are generally performed to probe chemical composition and elemental analysis of graphene materials and devices. One

particular advantage of the electron spectroscopic techniques, in general, and XPS, in particular, is their ability to reflect the local electrical potential: (1) developed as a result of charging due to photoelectron emission, and/or (2) externally applied electrical signal to the sample, since the kinetic energy of the emitted electron is directly affected by it. The latter has been extensively utilized to probe into chemically addressed electrical properties of materials and devices under operation by our group over the last 10 years.¹⁰

In real-life samples and devices, the graphene structures always contain morphological and structural defects that can be formed during growth and/or processing, which drastically affect the performance of graphene-based devices.¹¹ The chemical defects in graphene are generally referred to anything that changes the sp^2 carbon-hybridization. The amount and nature of defects depend on the synthesis method. However, such deviations from the ideal structure are not always unwelcomed for they can be useful, rendering new properties and potential applications. For instance, it was previously shown that defective graphene becomes chemically more reactive and magnetically susceptible with respect to oxidation, which makes the defective graphene a prospective magnetic carbon.¹² That is why large efforts have been made to further modify and functionalize its properties with controlled introduction of defects in graphene by exposing it to light, introducing foreign atoms or ions, etc.¹³⁻¹⁶

Since the properties of graphene are strongly related to the morphology, locating and understanding the nature of defects is vital for promoting its widespread applications.

^{a)}Electronic mail: suzer@fen.bilkent.edu.tr

Lucchese *et al.* proposed a method to quantify the density of disorder in graphene created by controlled doses of Ar^+ bombardment using Raman spectroscopy.⁷ A study of the evolution of Raman spectrum of graphene samples with different types and amount of defects has been recently reported for sp^3 type defects which were introduced by mild oxidation, vacancy-type defects produced by Ar^+ bombardment, and also for the defective pristine graphene produced by anodic bonding.¹⁷ They showed that the intensity ratio of the D to D' peak was around 13, decreased to 7 for vacancy-like defects, and reached a minimum of 3.5 for graphitelike structure. Another group reported the *in situ* electrical analysis of graphene transistor during etching with a helium ion beam.¹⁸ However, all of these studies focus on the atomic level defects and cannot give information about large defects on macroscopic level, which are mostly unavoidable for larger samples.

In this study, we employ different methodologies for detecting different types of large area structural/morphological defects and evaluating their effects on the electrical properties of the devices based on graphene films in an element-specific fashion by the application of external voltage bias while recording XPS data. Using the observed shifts in the C1s position, as a result of the applied bias, we previously showed that the electrical potential variations were uniform across the entire surface of a relatively defect free graphene layer, and not so uniform in an oxidized one, because of the morphological defects created by the oxidation process.¹⁹ In a recent publication, we used the method to reveal graphene–substrate interaction in graphene devices fabricated on the C- and Si-faces of SiC.²⁰ In this work, we use the method to study the nature of the defects on three different graphene surfaces some of which are created intentionally. As we will demonstrate below, our facile and controllable method amplifies further the appearance of morphological disorders and helps understand their role in electrical performance of the devices.

II. EXPERIMENT

Graphene layers used in the devices were grown on copper foils by chemical vapor deposition at 1035 °C under 10 Torr pressure. Partial pressures of CH_4 and H_2 gases were set as 3 and 7 Torr, and corresponding flow rates were 40 and 80 sccm, respectively. After the growth, the graphene layers were transfer-printed on commercial glass substrates and/or silicon wafers by using an S1813 photoresist (PR) as a mechanical support for graphene. This process is accomplished by spin coating graphene-copper foils with a thin layer of photoresist, and copper was completely etched away with FeCl_3 solution. After the etching step, the PR layer with graphene, applied on desired substrates, was heated to 80 °C to release the PR. Finally, the residues of PR layer were removed by dissolving in acetone. We used Raman spectroscopy to evaluate the quality and uniformity of the graphene samples. To intentionally oxidize the graphene layer, a single drop of 35% hydrogen peroxide (Merck, Darmstadt, Germany) is used in air. In order to apply an external bias,

two gold electrodes were fabricated using standard UV-photolithography and metallization technique.

XPS measurements were carried out using a Thermo Fisher K-Alpha photoelectron spectrometer with a monochromatic Al $K\alpha$ X-ray source. The instrument was slightly modified to allow the application of an external voltage of +6 V to the sample during data acquisition. The voltage was applied from one of the gold electrodes while the other one was grounded. The spectrometer is equipped with a low-energy flood-gun (FG) facility for charge neutralization, which is quite helpful in distinguishing between graphene covered and uncovered (bare glass surface) regions. The details of the FG parameters are given in the supplementary material.²² An Ar^+ ion gun was used to create intentional point and/or line defects on the sample with 3.5 μA beam current and spot size <500 μm . Raman spectra, which were obtained by a Witec Raman Spectrometer equipped with 532 nm laser, were also used to evaluate the equality of the transferred graphene and to monitor defects.

Three different samples to be presented below are chosen among the many we have studied over the years, to represent three different spectroscopic challenges. The details of the samples will be given at the appropriate places within the text.

III. RESULTS AND DISCUSSION

In many of the CVD grown graphene films on glass, we encounter ruptured regions (RGs) on the surface formed during transfer or other processes employed in fabricating devices. On the other hand, we also employ chemical oxidation and/or reduction locally or globally on graphene samples/devices. As a first demonstration of our methodology, we present a challenging XPS analysis of a sample containing both a RG and a large oxidized spot on the graphene layer on glass substrate, as schematically depicted in Fig. 1(a).

A. Charge-contrast XPS to locate and differentiate defects

In a typical analysis routine for locating defects, one usually employs XPS areal maps of C1s and O1s together as also shown in Fig. 1 for this sample, where the color bar reflects the intensity of the peaks. The inspection of the C1s areal map in the presence of low energy Flood Gun with 10 μA emission displayed in the upper graph of Fig. 1(b) shows a region with smaller carbon intensity, hinting the presence of a ruptured region. However, one must be cautious since carbon signal is observed in each and every sample due to the presence of adventitious carbon, even if no graphene is present. Hence, the analysis of C1s-signal only is not sufficient for validating the location of the RG. Two regions are observed to have larger O1s signal, the position of only one of which is negatively correlated with the C1s signal. Since the probe length of XPS is ~ 10 nm, O1s signal of the glass substrate is also observable; hence, the analysis of O1s-only is not sufficient either, due to the inability of distinguishing the chemical nature of O1s peak observed. At this point, we turn to the charging properties of different

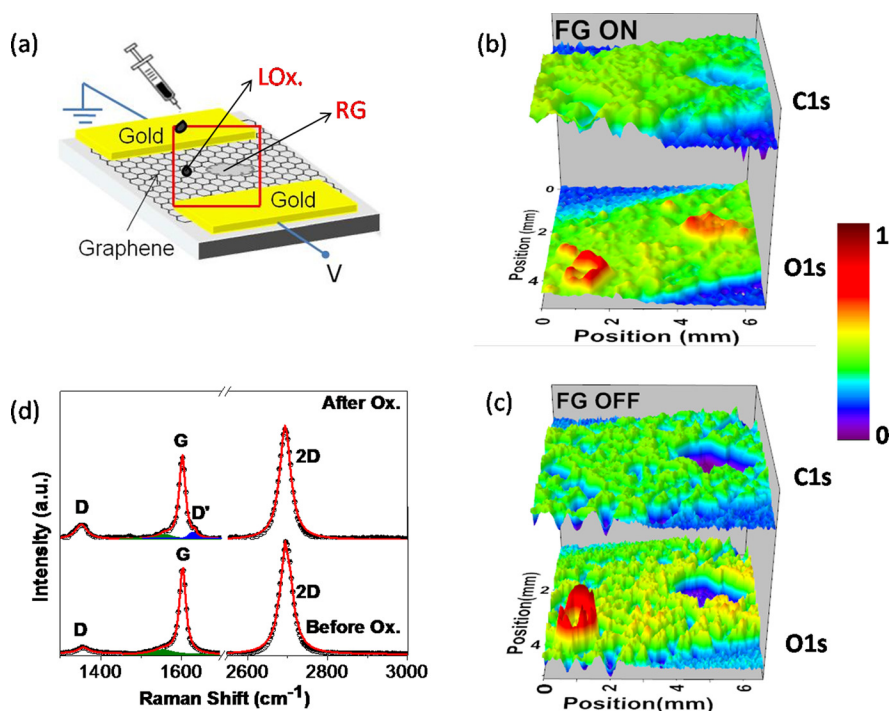


FIG. 1. (Color online) (a) Schematics of the sample and electrical connections. Areal maps of the intensity of C1s and O1s signals recorded with $100\ \mu\text{m}$ x-ray spot size; (b) with and (c) without the flood-gun. (d) Raman spectra of the region before and after chemical oxidation.

parts of the sample by disabling the charge compensation with the flood-gun, where C1s and O1s areal maps are shown in Fig. 1(c). As it is known, XPS analysis of insulator surfaces like glass is always difficult due to the charging, but luckily the presence of a thin layer of graphene enables one to investigate the insulating substrates, since graphene provides a blanket of conductivity, which was demonstrated in our previous study.¹⁹ Therefore, without charge compensation, the presence of the RG becomes apparent, because of the observation of very weak signal from both C1s due to lack of any graphene layer and O1s due to the charging of the sample, whereas the O1s signal is enlarged in the region where the chemical oxidation is performed. Therefore, the laterally determined negative correlation between the C1s and O1s signals, together with the charging property can successfully be used to locate and differentiate the above-mentioned two different types of morphological disorders.

Additional confirmation comes from the Raman spectra of the same sample recorded from the pristine and oxidized regions, as shown in Fig. 1(d). In the spectrum, the most intense features are the G band at $\sim 1600\ \text{cm}^{-1}$ and 2D band at $\sim 2700\ \text{cm}^{-1}$. The G band is due to Raman active doubly degenerate E_{2g} mode and the 2D band corresponds to overtone of the D band.²¹ Smaller intensity D band at $\sim 1350\ \text{cm}^{-1}$ is due to the second order of zone boundary phonons. For the defect free graphite or graphene layers, the zone boundary phonons are inactive due to the Raman fundamental selection rule, which is relaxed and activated in the defected graphene.^{5,21} D' is considered another defect induced feature which appears at $\sim 1620\ \text{cm}^{-1}$.⁵ Hence, the increase in the intensity of the D and D' bands in the spectrum after oxidation of graphene indicates introduction of further defects.

B. Voltage-contrast XPS to amplify defects

When conducting materials are subjected to current flow by use of a voltage bias, additional information is obtained from inspection of XPS peak positions. In Fig. 2(a), we display areal maps of C1s and O1s peak positions, recorded in the snap-shot mode of the instrument with $100\ \mu\text{m}$ x-ray spot size, when both electrodes are grounded and no current flows through the graphene layer(s) on a silicon oxide substrate. As seen from the figure, deviations in the C1s position is less than $0.1\ \text{eV}$ from its mean value of $284.7\ \text{eV}$ throughout the entire graphene surface having an overall resistance of $330\ \Omega$ of a pristine CVD grown graphene sample. Variations in the position of the O1s peak representing the substrate conform to the graphene overlayer and display also $\sim 0.1\ \text{eV}$ deviations from the mean value of $532.6\ \text{eV}$. In short, if no current is forced to flow, the graphene layer is perceived as an extremely smooth one, judging by the binding energies of C1s of the graphene layer, and also O1s of the substrate.

However, the appearance of morphological abnormalities are amplified, when the external bias is applied across the gold electrodes to induce the current flow, and the variations in the binding energy positions of the C1s and O1s peaks are displayed, as shown in Fig. 2(b). The increase in such variations is not only visible to the eye but can also be quantified by the computed standard deviations, as also given in the figure. The procedure of computing standard deviations is described in detail in the supplementary material section.²² Figure 2(c) shows the same areal maps after the sample was subjected to a mild oxygen plasma treatment, upon which the resistance jumps to $4\ \text{k}\Omega$. Detailed XP spectra of the C1s and O1s regions recorded in the conventional scanning mode of the slightly oxidized and pristine graphene are given in

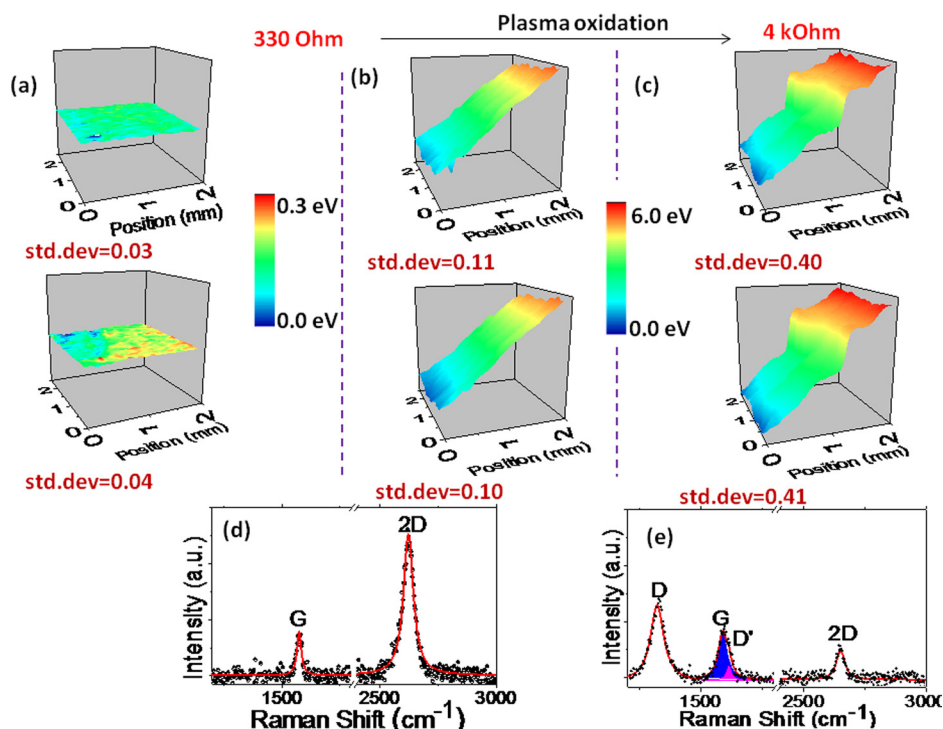


Fig. 2. (Color online) Areal maps of the measured binding energies of C1s and O1s with $100\ \mu\text{m}$ x-ray spot size as the device is grounded (a). Same device under the external bias before (b) and after the mild plasma oxidation (c) of the entire sample. Computed standard deviations for each case are also shown. The corresponding Raman spectra are given: (d) before and (e) after the mild oxidation.

the supplementary material section as Fig. S1.²² The increase in the resistance parallels the increase in the computed standard deviations from 0.1 to 0.4 for both the C1s and O1s peak positions, supporting the fact that the mild oxidation introduces sp^3 and other types of defects.^{4,5} The important result of such measurement is the utilization of voltage bias to amplify the otherwise hidden defect structures in the graphene layer. Another outcome is the visualization of the increased electrical resistance of graphene by the plasma oxidation, and semiquantitative correlation of it with the resultant larger local potential variations from the mean by the computed standard deviations. These findings are also corroborated with Raman measurements, shown in Figs. 2(d) and 2(e) for the pristine and the oxidized graphene samples, respectively. The pristine sample has only the G and 2D peaks, but after oxidation, D and D' bands appear again with a significant decrease in the intensity of 2D peak, and also a shift to higher frequency, in agreement with the results reported for oxidized sp^3 -defective graphene.^{4,5}

C. Ion gun to create defects and induce fatal performance

In the literature, the defects created by Ar^+ bombardment are referred as vacancylike defects, and the intensity changes of the Raman peaks for this type of disorder have been well studied.^{12,13} Therefore, another graphene device fabricated on a silicon oxide/silicon wafer was etched by the ion gun for the creation of additional defects. First, graphene was exposed to the Ar^+ ion beam directed to a point on the surface with 200 eV energy and for duration of 5 s, as illustrated

in Fig. 3(a). The formation of a circle-shaped defect is clearly evident in the small ($50\ \mu\text{m}$ x-ray spot size) areal mapped binding energy positions of both the C1s and O1s under the application of +6V to the device as shown in Figs. 3(b) and 3(c), respectively. Since the area is selected to be small for better visualization of the circular defects, the binding energy difference is only 3.0 eV in this range, but still a full 6.0 eV difference across the electrodes is measurable. On the other hand, an Ar^+ -bombardment along the line in the middle of the device creates a fatal line defect, resulting in a sharp voltage drop in the recorded peak positions of both the C1s and O1s peaks, as shown in Figs. 3(e) and 3(f). Surprisingly, after the creation of this fatal line defect, the resistance between the electrodes was measured as 6 k Ω . When C1s intensity and binding energy is recorded in the whole area of the device, instead of the created line wide as in Figs. 3(e) and 3(f), shown in Figs. 3(h) and 3(i), respectively, the passage of current around the fatal trenchlike defect region can be seen clearly, which explains the persistence of the finite resistance after all these treatments. Here again, the application of the voltage bias brings out the abnormalities, which can go undetected during conventional XPS analysis or by electrical-only characterization routes.

IV. SUMMARY AND CONCLUSIONS

In summary, we report on detection and investigation of different large structural imperfections of graphene layers by using different data collection modes of XPS. The control of charging properties of the insulating substrate using the flood-gun helps to distinguish between different types of

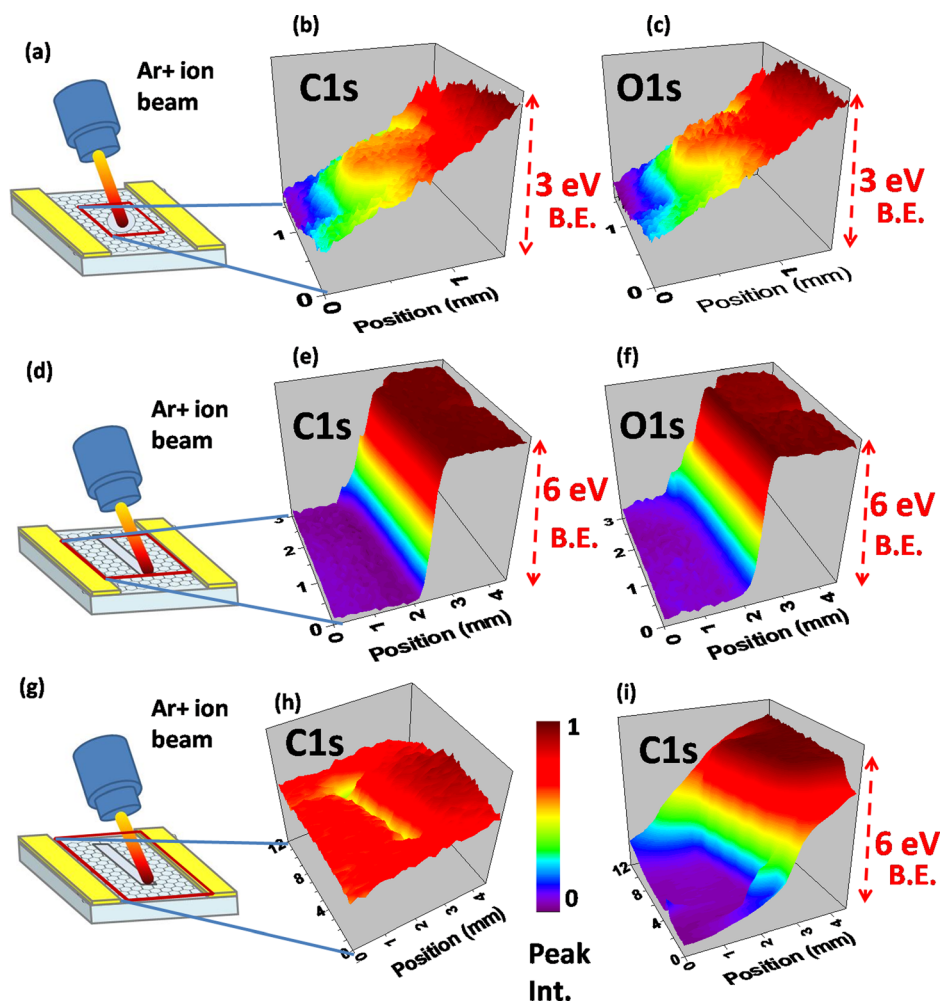


Fig. 3. (Color online) Schematic representations of (a) creating a point defect, (d) and (g) a line defect. Areal maps with $50\ \mu\text{m}$ x-ray spot size of the measured binding energies of the C1s (b) and O1s (c) peaks under an external bias of $+6\ \text{V}$ after creating a point defect, after creating a line defect (e) and (f). Areal map of C1s peak intensity (h) and binding energy position from the whole device area.

morphological defects. In addition, our experimental results with external bias give information of otherwise invisible defects and suggest that with increasing content of defects the binding energy deviations from the mean significantly increases. Overall, the simple variants of XPS described in this article provide new perspectives for obtaining vital information about type and shape of defect structures on graphene surfaces, and also on their effects to the electrical properties, which might be very useful for improving efficiencies of graphene devices used in electronics.

¹A. K. Geim and K. S. Novoselov, *Nat. Mater.* **6**, 183 (2007).

²K. S. Novoselov, D. Jiang, F. Schedin, T. J. Booth, V. V. Khotkevich, S. V. Morozov, and A. K. Geim, *Proc. Natl. Acad. Sci. U.S.A.* **102**, 10451 (2005).

³Y. M. Lin, C. Dimitrakopoulos, K. A. Jenkins, D. B. Farmer, H. Y. Chiu, A. Grill, and P. Avouris, *Science* **327**, 662 (2010).

⁴A. C. Ferrari, *Solid State Commun.* **143**, 47 (2007).

⁵A. C. Ferrari *et al.*, *Phys. Rev. Lett.* **97**, 187401 (2006).

⁶L. G. Cancado *et al.*, *Nano Lett.* **11**, 3190 (2011).

⁷M. M. Lucchese, F. Stavale, E. H. M. Ferreira, C. Vilani, M. V. O. Moutinho, R. B. Capaz, C. A. Achete, and A. Jorio, *Carbon* **48**, 1592 (2010).

⁸Z. H. Ni, W. Chen, X. F. Fan, J. L. Kuo, T. Yu, A. T. S. Wee, and Z. X. Shen, *Phys. Rev. B* **77** 115416 (2008).

⁹D. Graf, F. Molitor, K. Ensslin, C. Stampfer, A. Jungen, C. Hierold, and L. Wirtz, *Solid State Commun.* **143**, 44 (2007).

¹⁰H. Sezen and S. Suzer, *Thin Solid Films* **534**, 1 (2013).

¹¹I. L. Aleiner and K. B. Efetov, *Phys. Rev. Lett.* **97**, 236801 (2006).

¹²D. W. Boukhvalov and M. I. Katsnelson, *Nano Lett.* **8**, 4373 (2008).

¹³C. Stampfer, F. Molitor, D. Graf, K. Ensslin, A. Jungen, C. Hierold, and L. Wirtz, *Appl. Phys. Lett.* **91**, 241907 (2007).

¹⁴M. Kim, N. S. Safran, C. Huang, M. S. Arnold, and P. Gopalan, *Nano Lett.* **12**, 182 (2012).

¹⁵G. Compagnini, G. Forte, F. Giannazzo, V. Raineri, A. L. Magna, and I. Deretzis, *J. Mol. Struct.* **993**, 506 (2011).

¹⁶E. H. Martins Ferreira, M. V. O. Moutinho, F. Stavale, M. M. Lucchese, R. B. Capaz, C. A. Achete, and A. Jorio, *Phys. Rev. B* **82**, 125429 (2010).

¹⁷A. Eckmann, A. Felten, A. Mishchenko, L. Britnell, R. Krupke, K. S. Novoselov, and C. Casiraghi, *Nano Lett.* **12**, 3925 (2012).

¹⁸M. C. Lemme, D. C. Bell, J. R. Williams, L. A. Stern, B. W. H. Baugher, P. Jarillo-Herrero, and C. M. Marcus, *ACS Nano* **3**, 2674 (2009).

¹⁹C. Kocbas and S. Suzer, *Anal. Chem.* **85**, 4172 (2013).

²⁰P. Aydogan, E. Arslan, S. Cakmakyapan, E. Ozbay, W. Strupinski, and S. Suzer, *Appl. Phys. Lett.* **107**, 121603 (2015).

²¹F. Tuinstra and J. L. Koenig, *J. Chem. Phys.* **53**, 1126 (1970).

²²See supplementary material at <http://dx.doi.org/10.1116/1.4954401> for additional data and the procedure for computing standard deviations.